FOULING BY AQUEOUS SUSPENSIONS OF KAOLIN AND MAGNETITE: HYDRODYNAMIC AND
SURFACE PHENOMENA EFFECTS.

L. MELO and J.D. PINHEIRO
University of Minho - C.Q.P.A./INIC, 4700 Braga, Portugal

1. INTRODUCTION

When a suspension flows in contact with solid surfaces, the particles
it carries can be transported to the walls and, through a process of adhesion
form a more or less stable deposit. The basic phenomena of particulate
fouling include these two processes, together with the simultaneous removal
of the deposited particles. Knowledge of the mechanisms involved and also of
their mutual interference is essential to the qualitative as well as quanti-
tative characterization of different fouling situations.

The work reported in this text was based on experiments with kaolin-
-water suspensions, magnetite particles being also present in some cases.
Two major kinds of tests were performed: a) "Fouling tests", where the build-
-up of the deposit was continuously monitored through the measurement of lo-
cal heat transfer coefficients in an annular heat exchanger; b) "cohesion
tests", for the assessment of the "mechanical resistance" of the deposit,
which were carried out in an apparatus with two concentric cylinders, the
outer one being able to rotate at different velocities.

The paper also presents simple concepts and calculations that exemplify
two different approaches which are believed to be useful in fouling studies:
one is a more phenomenological (or "overall") approach based mainly on the
interpretation of the so-called "fouling-factor curves"; the other relies
upon a more detailed (or "microscopic") analysis of the individual processes
involved in the formation of the deposits (the adhesion process was used as
an example in this study). The two approaches agree in the interpretation of
several features of the experimental results. Although both approaches need
to be substantially developed (particularly in mathematical terms), they
seem to have a potential for practical applications in the prediction of
fouling tendencies.

2. EQUIPMENT AND EXPERIMENTAL METHODS
2.1. Annular heat exchanger

This test section is 2 meter long and is composed by an inner copper
tube, easily removable, and an external perspex tube (diameters: 25mm and
36mm respectively). Thermocouples are located on the internal wall of the
inner tube, as well as in the fluid at positions A,B,C,D and E (Figure 1).
The pressure drop is measured with a differential manometer, allowing the
calculation of friction factors to be made. The heat flux, provided by an
electrical resistance placed inside the copper tube, is determined from
continuous recording of voltage and current intensity. Local thermal resis-
tances of the deposits (fouling resistances) at the different positions can
be then calculated as described elsewhere (1). The annular heat exchanger is
inserted in a closed loop circuit containing a stirred cooling tank (250
liters) and PVC tubes of 25mm diameter (Figure 2).

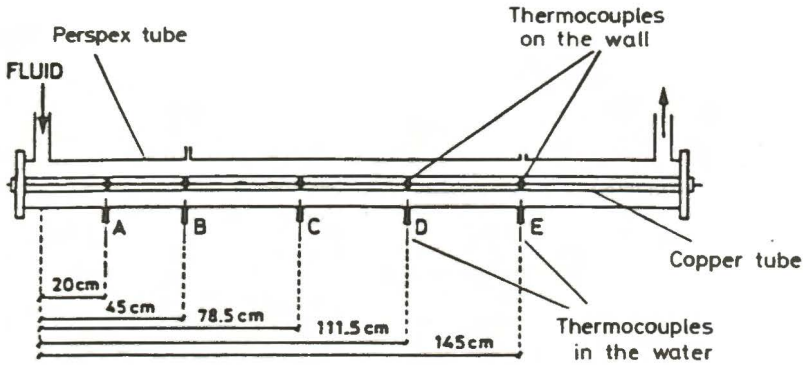Several fouling tests were run with the kaolin suspension flowing at

FIGURE 1 - Annular heat exhanger

Reynolds numbers (based on the equivalent diameter of the annulus) between 2300 and 11000, using a constant heat flux of about 3000 W/m^2, pH=7.5, bulk water temperature = 12ºC and kaolin concentration = 2.2 Kg/m^3. The final thickness of the deposit was measured with a micrometer-based device.

Tests with a magnetite suspension and with a mixed kaolin-magnetite suspension were also carried out (only at Re = 6900).

2.2. Rotating cylinder apparatus

This equipment is composed by a removable inner copper tube (which in the present study was made of samples of the fouled copper tube obtained in the heat exchanger tests) and a 36 mm diameter perspex outer tube, 8 cm long (Figure 3). The latter is connected to an alternating current motor with
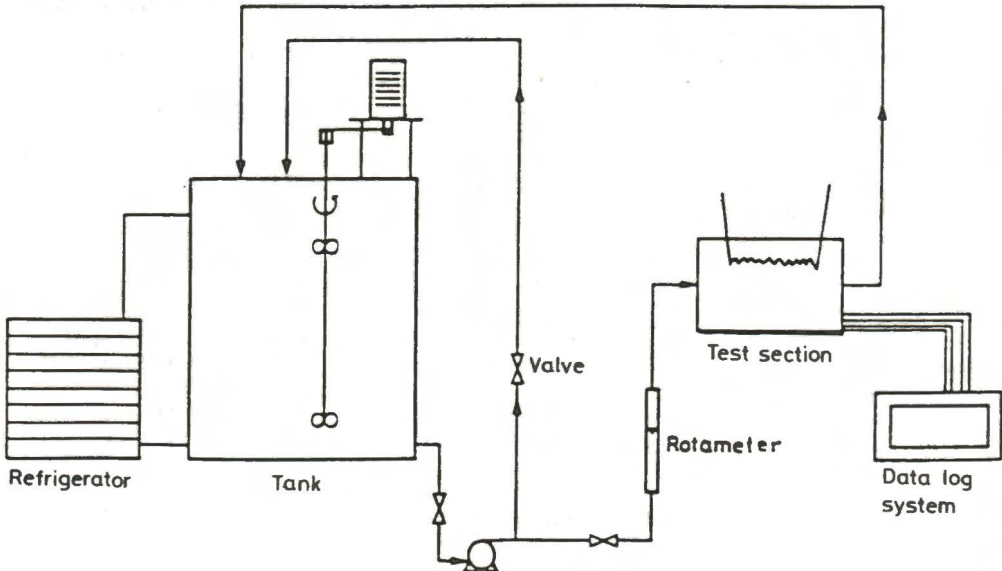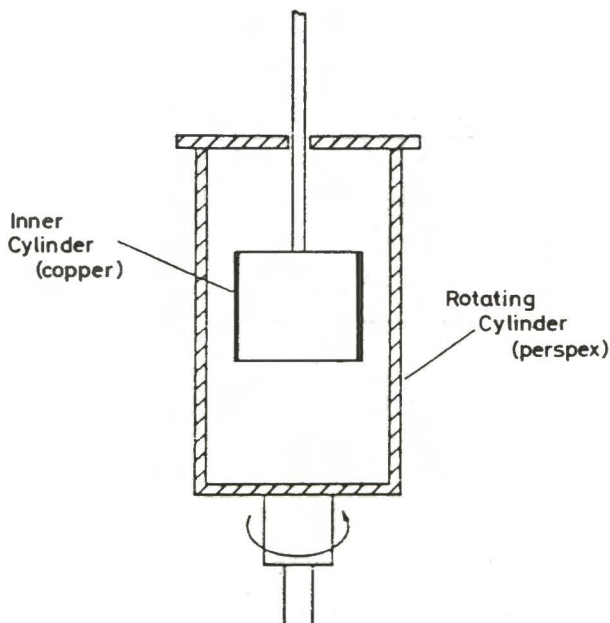

FIGURE 2 - Fouling test rig

Figure 3. – Rotating cylinder apparatus

controlled input voltage. The velocities of rotation of this cylinder were measured with a stroboscope.

The fouled samples (2 cm long) were dried, weighed and placed inside the apparatus after filling it with water at pH 7.5. After about one hour, the outer tube was rotated at a low velocity for 3 minutes, the fouled inner cylinder was removed, dried and weighed. This technique was repeated several times using higher and higher rotating speeds.

2.3. Particles

A laser flow granulometer and a scanning electron microscope were used to characterize the geometric features of the kaolin and magnetite particles.

The kaolin particles are roughly similar to discs of 16 microns diameter and 1 micron thickness (average values), corresponding to an equivalent diameter of 7 microns (the diameter of the sphere with a volume equal to that of the particle). The particles in the deposit seem to adhere to each other bu their larger faces. Their surfaces, however, are very irregular which makes the contact area much smaller than if they were smooth flat plates.The density of kaolin is 2600 Kg/m^3.

The shape of the magnetite particles, although irregular, is more similar to the shape of a sphere or of a cube, and their average diameter is ·21 microns. The density of magnetite is 5200 Kg/m^3.

The electrokinetic ("zeta") potential of the kaolin and magnetite particles at several pH values was obtained from electrophoresis measurements using a "zetameter" apparatus (Figure 4). At pH 7.5, the zeta potential is about – 0.05 V for kaolin and –0.04 V for magnetite, both bearing negative
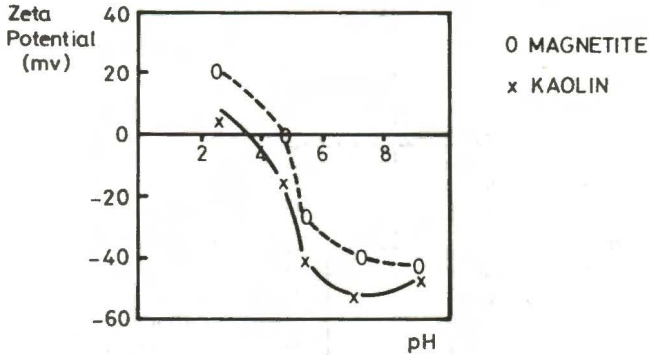
Figure 4. Zeta potentials of kaolin and mangetite

surface charges.

3. FOULING TESTS AND THEIR INTERPRETATION

3.1. Fouling Models

The data from the "fouling tests" were studied in two stages. First, the basic model of Kern and Seaton (2) was fitted to the experimental fouling curves in order to obtain values of the deposition flux ($\emptyset_d$) and of the asymptotic fouling resistance (R_f^{∞}). Then, the processes controlling the deposition flux were identified and characterized on the basis of a more detailed model such as the one of Pinheiro (3,4).

Assuming that fouling occurs as a result of the competition between a deposition flux ($\emptyset_d$, constant with time) and a removal flux ($\emptyset_r$, increasing with time), Kern and Seaton derived the asymptotic fouling equation:

$$R_f = R_f^{\infty} \ [1-\exp \ (-\beta t)] \qquad (1)$$

where:

$$R_f^{\infty} = \emptyset_d \ / \beta \qquad (2)$$

and:

$$\beta = \emptyset_r \ / R_f \qquad (3)$$

Parameter β is supposed to be directly proportional to the wall shear stress (i.e., to the square of the average fluid velocity), and its reciprocal ($1/\beta$) can be regarded as a measure of the cohesion of the deposit in a given hydrodynamic environment.

The model of Pinheiro brings together the ideas expressed by Taborek et al (5), Watkinson and Epstein (6) and Crittenden and Kolackzkowski (7) about the deposition and removal terms of Kern and Seaton's equation. In the case of particulate fouling, deposition is considered to be the result of two processes occurring in series – the transport of particles to the deposition surface and their interaction at this surface (adhesion):

$$\emptyset_d = \frac{C_b}{\rho_f \ K_f \ [\ (1/K_t) + (1/K_a) \ ]} \qquad (4)$$

ρ_f and K_f are the density and the thermal conductivity of the deposit: C_b is the bulk suspension concentration. K_t, the mass transfer coefficient, is dependent on $\sqrt{f} \cdot \bar{v}$ for turbulent diffusion. The adhesion coefficient, K_a, will tend to decrease as the velocity increases and Pinheiro suggested that it should be proportional to $(\bar{v})^{-b}$. f is the friction factor, $\bar{v}$ the average fluid velocity and b an empirical parameter that changes with the type of mechanism that controls the deposition process.

For lower fluid velocities, the mass transfer rate can be much slower than the adhesion rate ($K_t \ll K_a$), implying that the former will be the controlling step. Then:

$$\emptyset_d \simeq \emptyset_t = \frac{K_t \quad C_b}{\rho_f \quad k_f} = \frac{K_1 \sqrt{f} . \bar{v} \, C_b}{\rho_f \quad k_f} \qquad (5)$$

where $\emptyset_t$ is the transport flux and $b \longrightarrow 0$.

If $K_t \gg K_a$, the deposition rate will be governed by the adhesion flux ($\emptyset_a$) that decreases as the velocity increases:

$$\emptyset_d = \emptyset_a = \frac{K_a \quad C_b}{\rho_f \quad K_f} = \frac{K_2 \, C_b}{\bar{v}^b . \rho_f . K_f} \qquad (6)$$

with $b > 0$, approaching 1.

The fluid velocity is considered to affect the removal flux in two ways: and increase in $\bar{v}$ produces a higher shear stress but, at the same time, tends to create more compact deposits. Thus, $\emptyset_r$ will be not only proportional to $f . \bar{v}^2$ but will also vary inversely with $\bar{v}^a$, a being an empirical parameter related to the cohesion of the deposit.

Equation 3 can be written as:

$$\emptyset_r = K_3 \, f \, (\bar{v})^{2-a} \, R_f \qquad (7)$$

Pinheiro suggested also that the greater the fraction occupied by the "loose" layers in the deposit, the greater will be $\emptyset_r$. A "hard" deposit will then have a high $1/\beta$ ("mechanical resistance" or "cohesion") and a low fraction os "loose" material.

3.2. Results and Discussion

3.2.1. Tests with pure kaolin suspensions.
The "fouling tests" produced curves of R_f versus t (time) for different Reynolds numbers. Values of R_f^∞, $\emptyset_d$ and β were obtained from the fitting of Equation 1 to these data (Figures 5 to 7). It had previously been observed (8) that for the lower range of Reynolds numbers, positions A, B and C are in an entrance zone characterized by a developing laminar layer where the deposits are much thicker, as shown in Figure 5.

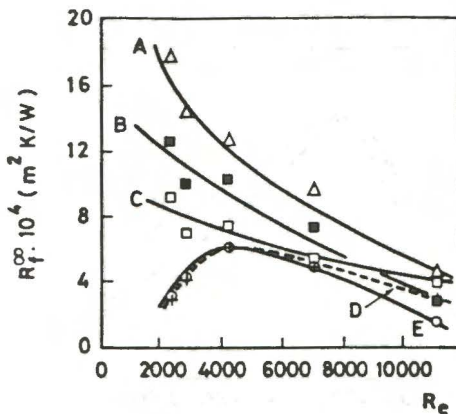It appears that particle transport will be the process controlling

Figure 5. Asymptotic thermal resistance

deposition for Re less than about 4000 ($\emptyset_d = \emptyset_t$). The mass transfer mechanism is expected to be turbulent diffusion, because the dimensionless relaxation time, given by:

$$t_p^+ = \frac{(v^*)^2 \cdot \rho_P D_p^2}{18 \mu \upsilon} \qquad (8)$$

is much smaller than 0.1, for the kaolin particles in this range of Reynolds numbers ($t_p^+ < 0.015$). In fact, for $2300 < Re < 3850$, the average dependence of $\emptyset_t$ ($\approx\emptyset_d$) on Re, obtained from Figure 6 is (9):

$$\emptyset_d \sim Re^{0.73} \qquad (9)$$

quite similar to the dependence usually found when turbulent diffusion mechanisms are present. It should be stressed that the increase in R_f^{∞} with Re is due to the increase not only in $\emptyset_d$ but also in the relative cohesion of the deposit, as shown in Figure 7. For this case, parameter a of Pinheiro's model was found to have a value of 2.4 (1), indicating that the increase in the "mechanical strength" of the deposit is higher than the increase in the fluid shear stress.

For $Re > 4000$, a change of control seems to occur, as shown by the gradually decreasing values of $\emptyset_d$. Here, adhesion is the slower process, therefore determining the rate of deposition ($\emptyset_d \approx \emptyset_a$), with b ≈ 1 (1).

Changes of control were also observed by other authors in particulate and precipitation studies (6, 10, 11).

3.2.2. <u>Tests with magnetite particles</u>. A pure magnetite suspension and a mixed kaolin-magnetite suspension were used in two fouling tests with Re = 6900 and pH = 7.5. The magnetite concentration was 0.3 Kg/m^3 in both tests and the kaolin concentration was kept at 2.2 Kg/m^3. Table 1 compares the data from these two runs with those obtained using only kaolin at the same Reynolds number and pH. The deposition flux ($\emptyset_d$) was reduced in the presence of magnetite, and the deposit cohesion ($1/\beta$) was increased. The fact that tp+> 0.1 for the magnetite particles suggests that the transport process will probably be determined by an inertial mechanism (12), resulting in higher values of the transport flux. In fact, if a particle transport model such as that of C. N. Davies (13, 14) is used to estimate the mass transfer flux (J_t) for the pure kaolin and the pure magnetite suspensions, substantially greater values are obtained in the second case:

$$J_t \text{ (pure kaolin)} = 7.7 \cdot 10^{-8} \text{ Kg/m}^2\text{s}$$
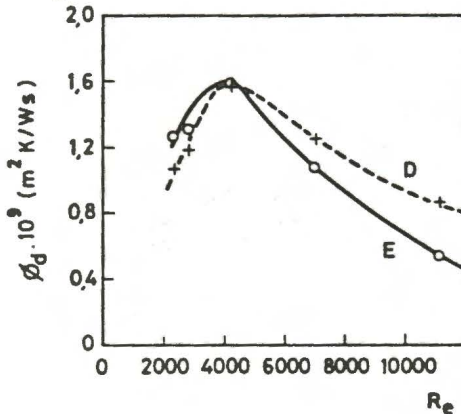$$J_t \text{ (pure magnetite)} = 5.4 \cdot 10^{-6} \text{ Kg/m}^2\text{s}$$
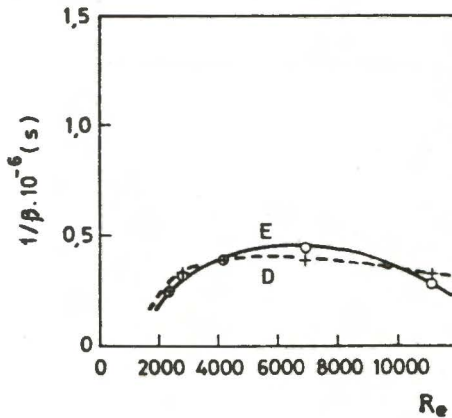

Figure 6. Deposition flux

Figure 7. "Resistance to removal" of the kaolin deposits

Obviously, if mass transfer were the governing step, the experimental deposition flux would show higher values for the magnetite deposits, which was not the case. This leads to the assumption that adhesion was also the controlling process during magnetite deposition at Re = 6900. Therefore, the conclusion from Table 1 is that the adhesion process is "more difficult" (or "slower") in the formation of pure magnetite deposits than in the formation of pure kaolin deposits.

Note that in spite of the higher total concentration of particles in the kaolin/magnetite experiments, the fouling rate is again lower than in the pure kaolin tests. The values of R_f for t = 10 days confirm the slowness of the fouling process when there are magnetite particles in suspension.

4. BASIC STUDY OF THE ADHESION FORCES IN THE DEPOSITS

4.1. Theory and Equations

In the case of particulate deposition, the physical forces of adhesion (mainly van der Waals and electrostatic forces) seem to play the more important role since it is supposed that no chemical reactions or phase changes are involved in the buid-up of these deposits. While van der Waals forces are almost always attractive, the electrostatic double-layer forces originate repulsion effects when the surface charges of the particles are of the same sign (as is the case in this study). Equations for the calculation of these forces are presented below in order to show the potential

Table 1. - Results with suspensions containing magnetite(fully developed flow region)

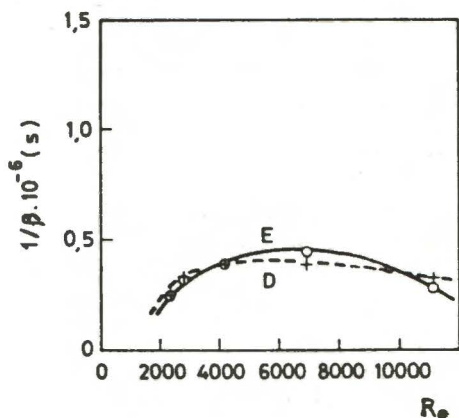| Re	Suspended Particles	$R_f^{\infty} \cdot 10^4$ $(m^2 K/W)$	Y_f (microns)	$\emptyset_d ; 10^9$ $(m^2 K/J)$	$(1/\beta) \cdot 10^{-6}$ (seconds)	R_f for $t=10$days
	Kaolin($2.2Kg/m^3$)	5.0	81	1.19	0.42	$4.4 \cdot 10^{-4}$
6900	Magnetite($0.3Kg/ /m^3$)	3.9	76	0.79	0.42	$3.2 \cdot 10^{-4}$
	Kaolin($2.2Kg/m^3$) +Magnetite($0.3Kg/ /m^3$)	5.0	69	0.75	0.66	$3.6 \cdot 10^{-4}$

Figure 7. "Resistance to removal" of the kaolin deposits

Obviously, if mass transfer were the governing step, the experimental deposition flux would show higher values for the magnetite deposits, which was not the case. This leads to the assumption that adhesion was also the controlling process during magnetite deposition at Re = 6900. Therefore, the conclusion from Table 1 is that the adhesion process is "more difficult" (or "slower") in the formation of pure magnetite deposits than in the formation of pure kaolin deposits.

Note that in spite of the higher total concentration of particles in the kaolin/magnetite experiments, the fouling rate is again lower than in the pure kaolin tests. The values of R_f for t = 10 days confirm the slowness of the fouling process when there are magnetite particles in suspension.

4. BASIC STUDY OF THE ADHESION FORCES IN THE DEPOSITS
4.1. Theory and Equations

In the case of particulate deposition, the physical forces of adhesion (mainly van der Waals and electrostatic forces) seem to play the more important role since it is supposed that no chemical reactions or phase changes are involved in the buid-up of these deposits. While van der Waals forces are almost always attractive, the electrostatic double-layer forces originate repulsion effects when the surface charges of the particles are of the same sign (as is the case in this study). Equations for the calculation of these forces are presented below in order to show the potential

Table 1. - Results with suspensions containing magnetite(fully developed flow region)

Re	Suspended Particles	$R_f^{\infty} \cdot 10^4$ $(m^2 K/W)$	Y_f (microns)	$\emptyset_d \cdot 10^9$ $(m^2 K/J)$	$(1/\beta) \cdot 10^{-6}$ (seconds)	R_f for $t = 10 days$
	Kaolin(2.2Kg/m^3)	5.0	81	1.19	0.42	4.4 .10^{-4}
6900	Magnetite(0.3Kg/m^3)	3.9	76	0.79	0.42	3.2 .10^{-4}
	Kaolin(2.2Kg/m^3) +Magnetite(0.3Kg/m^3)	5.0	69	0.75	0.66	3.6 .10^{-4}

usefulness of a more detailed interpretation of the adhesion process. A deeper theoretical understanding of the phenomenon is available in this book and elsewhere (15, 16, 17, 18).

4.1.1. <u>van der Waals Forces</u>. In the case of two different spherical particles of radii R_1 and R_2, these attractive forces can be estimated by:

$$F_A = \frac{A' \; R_1 \; R_2}{6(R_1+R_2) \; H^2} \qquad (10)$$

where H is the separation distance between the two particles and A' is the Hamaker constant. For two particles of the same material $\underline{1}$ in vacuum, the Hamaker constant is given by (16, 18):

$$A_{1\;1} = \frac{3}{4} \; \pi^2 \; N_1^2 \; I_1 \, \alpha_1^2 \qquad (11)$$

N_1 is the number of molecules per unit volume, I_1 is the ionization potential of the material and α_1 is the polarizability of the material given by (19):

$$\alpha_1 = \frac{3}{4 \, \pi \, N_1} \; \frac{n_1^2 - 1}{n_1^2 + 2} \qquad (12)$$

n_1 being the refractive index of the material.

For two particles of different substances (1 and 2) immersed in a third medium (substance 3), the Hamaker constant will be:

$$A_{132} = (\sqrt{A_{11}} - \sqrt{A_{33}}) \cdot (\sqrt{A_{22}} - \sqrt{A_{33}}) \qquad (13)$$

If substances 1 and 2 are the same, the last expression results in :

$$A_{131} = A_{11} + A_{33} - 2 \sqrt{A_{11} \, A_{33}} \qquad (14)$$

4.1.2. <u>Electrostatic Double-Layer Forces</u>. Phenomena such as the dissociation of surface groups and the adsorption of ions from the liquid phase tend to create charges on the surfaces of the particles. In order to maintain the overall system electrically neutral, oppositely charged solution ions concentrate near the solid surfaces. Each particle will then have its own electrostatic double-layer that may interact with similar double-layers of other particles.

For two different particles, 1 and 2, immersed in a liquid, the double--layer force is (20):

$$F_R = - \frac{\varepsilon \; R_1 R_2 (\Psi_{01}^2 + \Psi_{02}^2) \cdot \exp(-H/\delta)}{2 \; (R_1+R_2) \cdot \delta \cdot [1-\exp(-2H/\delta)]} \left\{ \frac{2 \; \Psi_{01} \; \Psi_{02}}{\Psi_{01}^2 + \Psi_{02}^2} - \exp(-H/\delta) \right\} \qquad (15)$$

ε is the dielectric constant of the liquid. Ψ_{01} and Ψ_{02} can be considered to be similar to the zeta potentials of particles 1 and 2, and δ is the thickness of the double layer. This equation is reasonably valid for values of Ψ_{01} and Ψ_{02} less than 50–60 mV (20) and for double-layer thicknesses that are small compared to the particle size ($R > 10.\delta$). The thickness of the double-layer (δ) is given by:

$$\frac{1}{\delta^2} = \frac{\cdot 4 \; e^2}{\varepsilon \; K_B \; T} \qquad (z_i^2 \; n_{io}) \qquad (16)$$

$e = 1.6 \cdot 10^{-19}$ Coulomb is the charge of the electron, K_B is the Boltzmann constant ($1.3805 \cdot 10^{-23}$ J/K), z_i is the valency of ion $\underline{i}$ and n_{io} is the number of ions $\underline{i}$ per unit volume of the liquid. In the case of water, $\varepsilon = 717.10^{-12}$ (Coulomb)^2/Nm^2 and $z_i = 1$ or -1.

4.1.3. <u>Force of Adhesion and Potential Energy of Interaction</u>. The resultant adhesion force (F_T) is the sum of the two forces described above:

$$F_T = F_A + F_R \qquad (17)$$

although a few other contributions to the overall bond effect could be considered (21, 22, 23). The potential energy of interaction (V_T) and the force of adhesion are related by:

$$F_T = \frac{dV_T}{dH} \qquad (18)$$

Figure 8 shows the typical shape of the Potential Energy of Interaction versus Distance curve for the case of two solids with surface charges of the same sign (15) (Bohr repulsions at very short distances are also considered in this schematic representation).

The distance at which adhesion occurs has an outstanding effect on the intensity and stability of the interactions between the two bodies. For instance, particles depositing in a secondary minimum can be more easily removed than those stabilized in a primary minimum.

The existence of an energy barrier makes adhesion more difficult and can explain why in some situations this process controls the deposition rate. In fact, as Rajagopalan and Kim (24) noted in the cases where an energy barrier exists, an increase in the fluid velocity originates a decrease in the concentration of the particles at the secondary minimum, due to; i) the relatively weak adhesion force that makes removal more efficient; ii) the difficulty of the particles to overcome the energy barrier. The result is that the deposition flux will decrease with higher velocities, meaning that it is controlled by the adhesion process.

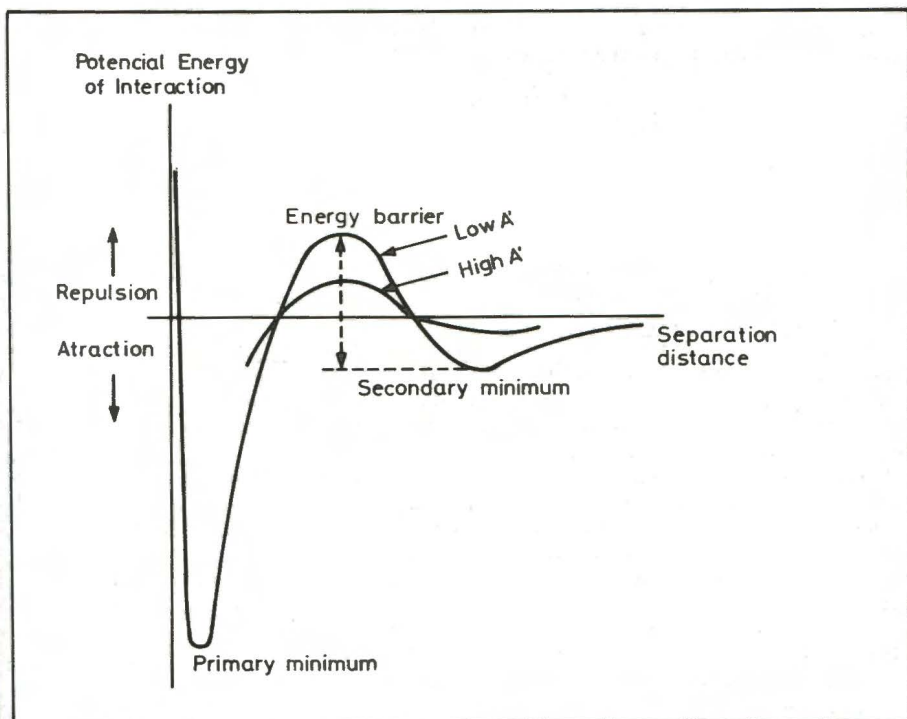The shape of the curve of Figure 8 depends on various factors, such as

Figure 8 - Potential energy of interaction

the ionic strength of the solution, the surface charge potential (pH effects included) or the value of the Hamaker constant (21, 22, 25). In particular, a greater Hamaker constant tends to decrease the height of the energy barrier and to flatten the secondary minimum (21, 22).

4.1.4. Hydrodynamic force in the rotating apparatus. In a concentric cylinder apparatus with a rotating outer tube the relationship between the wall shear stress (τ_w) and the angular velocity (ω) can be obtained from the following correlation developed by Wendt (17, 26):

$$\tau_w = 0.5\varrho \cdot \omega^2 R_0{}^2 \ 0.0013 \ [0.04 + (R_i/R_0)^{10}] \qquad (19)$$

where ϱ is the density of the liquid and R_i and R_0 are the inner and outer radii of the annulus, respectively.

Assuming that the particles deposited on the inner surface of the annulus are located in a laminar sub-layer, the hydrodynamic force (F_H) exerted by the fluid on them can be estimated by:

$$F_H = \frac{C_D v^2 \varrho A_p}{2} \qquad (20)$$

where A_p is the projected area of the particle (perpendicular to the direction of flow), v is the local fluid velocity and C_D is the drag coefficient ($= 24/Re_p$ in the Stokes regime). Re_p is the particle Reynolds number based on the particle equivalent diameter (D_p) and on the local fluid velocity at a distance equal to the half-thickness of the particle. The expression of the universal velocity profile in the laminar sublayer is:

$$v = Y (\tau_w / \mu) \qquad (21)$$

If $Y = Y_c$, the half-thickness of the particle (i.e., the distance of the adhesion surface to the center of the particle), Equation 20 will give:

$$F_H = \frac{12 Y_c \tau_w A_p}{D_p} \qquad (22)$$

The work of Visser (16, 17, 18) showed that the numerical values of the adhesion and hydrodynamic forces are identical, that is:

$$F_T = F_H \qquad (23)$$

which enables the experimental determination of the adhesion force by carrying out tests in this type of rotating apparatus.

4.2. Results and Discussion

4.2.1. Kaolin deposits. a) The two-layer structure of the deposits. Figure 9 presents the results found in the rotating cylinder apparatus using samples of copper tubes fouled by kaolin-water suspensions. These deposits were obtained in the developed flow region of the annular heat exchanger at the Reynolds numbers, $(Re)_{h.e.}$, indicated in the Figure.

As expected, the mass of deposit removed from the sample tube increased with the velocity of rotation, that is, with the hydrodynamic force exerted by the water. However, all the curves show a clear transition point that separates an easily removable portion of the deposit from a very cohesive layer. The results confirm the existence of layers with different adhesion characteristics within the same deposit, the outer ones being rather "loose" and the inner ones much more "rigid" or "hard".

Note that the mass percentage of "hard" inner layer goes from 50% to 70% and that this layer is practically not removable even at high velocities. The increase in the mass percentage of hard layer from Re=2300 to Re=4140 is substantial and may explain the increase in R_f with the Reynolds number at the lower velocity range; it constitutes also an argument to support the assumptions included in the removal term of Pinheiro's model.
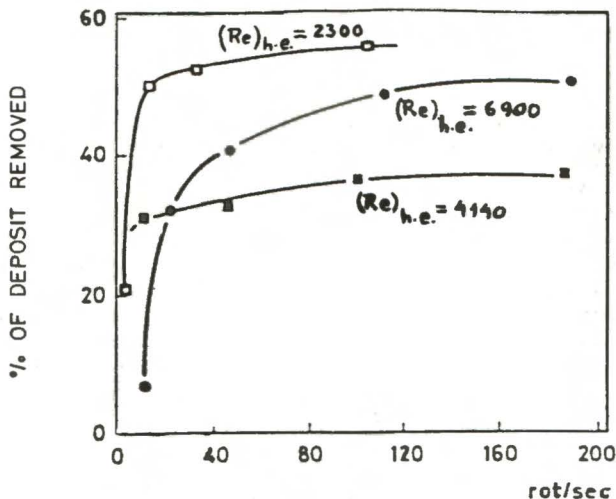
Figure 9. – Mechanical resistance of the kaolin deposits

In the case under study, Equation 19 can be written as:

$$\tau_w = 5.5 \cdot 10^{-4} \, n_r 2 \qquad (24)$$

where n_r is the number of rotations per second (r.p.s.).

The shear stress in the annular heat exchanger, $(\tau_w)_{h.e.}$, can be estimated by:

$$(\tau_w)_{h.e.} = \frac{f \, \varrho \, \bar{v}^2}{2} \qquad (25)$$

where f is the Fanning friction factor (obtained from pressure drop measurements). For equal values of the two shear stresses (Equations 24 and 25), the following values of the velocity of rotation are obtained: 29 rps for Re = 2300; 52 rps for Re = 4140; 78 rps for Re = 6900, showing that the hydrodynamic force acting in the annular heat exchanger could not remove the inner layer of the kaolin deposits, but was able to affect the outer "loose" layer quite easily.

The fact that particles can deposit in the primary minimum or in the secondary minimum offers some explanation for the existence of a "hard" and a "loose" layer in the same deposit. If the particles in the outer layers remain on the deposit for a sufficient time, they can be gradually "pressed" against the inner layers as the deposit grows, thereby increasing their probability of reaching the stable primary minimum. Other authors (27) suggest that in some cases the adhesion between solid surfaces may increase with time due to the slow reorientation of electrical charges at the surfaces. This could happen in the inner layers of a deposit since they are not being affected by the hydrodynamic removal forces.

b) <u>Approximate calculation of the adhesion forces</u>. The Van der Waals force can be roughly estimated as a function of the separation distance considering the following kaolin properties: molecular weight = 242; refractive index = 1.56; density = 2600 Kg/m^3; $N_1 = 6.47 \cdot 10^{27}$ molecules/m^3 and $I_1 = 9.58 \cdot 10^{-19}$ Joules per molecule (the ionization potential of aluminium). The value obtained for the Hamaker constant of kaolin was:

$$A_{11} = 4.20 \cdot 10^{-20} \text{ J}$$

The polarizability of water is (19):

$$\alpha_3 = 1.44 \cdot 10^{-30} \text{ m}^3$$

giving:

$$A_{33} = 3.76 \cdot 10^{-20} \text{ J}$$

Thus, when two kaolin particles interact in water:

$$A_{131} = 1.21 \cdot 10^{-22} \text{ J}$$

Precise values of the separation distance between the kaolin particles in water are not known. According to Grim (28) and Norrish (29), an almost--crystalline water layer is formed between clay particles, its thickness varying from a few angstroms to hundreds of angstroms, depending on the swelling properties of these minerals. In the case of kaolinite, swelling is much less pronounced than in other clay minerals such as montmorillonite. Thus, it is not unreasonable to assume a particle separation distance of the order of 10 Angstroms for kaolinite, this being a common value of the thickness of the crystalline water interlayer when swelling is not significant (29).

Although the kaolin particles are similar to discs, their surfaces are far from being smooth and the contact between two neighbouring particles is probably established at one or two points. Assuming that there is only one point of contact, the sphere-sphere approach can be roughly used replacing the diameter of the sphere by the thickness of the kaolin particles (1μ m). Considering that each particle in the deposit is surrounded by eight other particles, Equation 10 gives, for H = 10 Å :

$$F_A = 4.0 \cdot 10^{-11} \text{ N}$$

The electrostatic double-layer force can be estimated using the value of the zeta potential at pH 7.5 obtained from Figure 4. The thickness of the double-layer is (Equation 16):

$$\delta = 1.54 \cdot 10^{-7} \text{ m}$$

considering that the only ions in the liquid are H^+ and OH^-. Then (Eq.15):

$$F_R = -1.2 \cdot 10^{-11} \text{N}$$

and the resultant adhesion force will be:

$$F_T = 2.8 \cdot 10^{-11} \text{ N}$$

On the other hand, the hydrodynamic force exerted on the kaolin deposit in the rotating cylinder tests can be calculated from Equation 22, taking into account that for the kaolin particles $A_p = 16 \cdot 10^{-12} \text{ m}^2$, $Y_c = 0.5 \cdot 10^{-6}$ m and $D_p = 7.3 \cdot 10^{-6}$ m, giving:

$$F_H = 7.26 \cdot 10^{-15} \text{ n}_r^2$$

The equality between F_T and F_H implies that:

$$n_r = 62 \text{ rps}$$

which seems to be a very reasonable value when compared with the results shown in Figure 9.

4.2.2. Deposits with magnetite. The kaolin-magnetite deposit obtained in the annular heat exchanger with Re = 6900 showed a stronger "mechanical resistance" than the pure kaolin deposit formed at the same operating conditions (cf. Figures 9 and 10): the "hard" inner layer of the mixed deposit represents 80% of the total mass of the deposit, against about 50-60% for the pure kaolin situation. From the results of Table 1, it appears that the rate of adhesion in the mixed deposit is lower than in the pure kaolin deposits, although at the same time the adhesion forces are stronger.
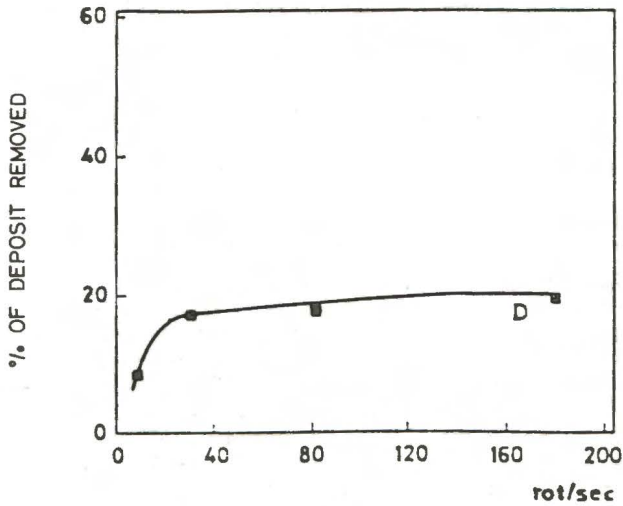
Figure 10. – Mechanical resistance of the kaolin-magnetite deposit

a) Approximate calculation of the adhesion forces. It is highly probable
that a significant part of the interactions in these deposits will occur
between kaolin particles, due to the greater concentration of this material
in the suspension. Nevertheless, there is a clear indication that the
presence of magnetite affects the overall system, and even a rough estimate
of the adhesion forces between the two types of particles may lead to a
better understanding of the synergic effects already detected.

Magnetite has the following properties: molecular weight = 232;
refractive index = 2.42; density = 5200 Kg/m^3; N_2 = 1.35 $.10^{28}$ molecules/m^3;
I_2 (ionization potential of the iron) = 7.19 $.10^{-19}$ J/molecule. The Hamaker
constant of magnetite will be :

$$A_{22} = 11.5 .10^{-20} J$$

while for kaolin plus magnetite particles immersed in water this parameter
has the following value:

$$A_{132} = 0.28 .10^{-20} J \qquad (26)$$

The Van der Waals force is then given by:

$$F_A = \frac{2.23 .10^{-28}}{H^2}$$

In the case of surfaces with dissimilar zeta potentials, the lower one
(that of magnetite, 0.04 V) appears to determine the intensity of the
repulsive forces (16).

There are however no indications about the probable distance of inter-
action (H) between the particles of magnetite and of kaolin, but the order
of magnitude of the overall adhesion force (F_A) can be seen in Table 2, as-
suming that each magnetite particle is surrounded by five kaolin particles.
The theoretical values given by Equation 26 and in Table 2 are much greater
than those obtained for the pure kaolin deposit, showing a qualitative
agreement with the experimental results presented in Figures 9 and 10.

b) Interpretation of the results. At first sight, the higher cohesive forces
in the mixed deposit seem to be in contradiction with its lower rate of
adhesion (or the increased difficulty of adhesion). This could be
tentatively explained by the fact that the Hamaker constant is 23 times

Table 2. – Adhesion forces between kaolin and magnetite particles

Interaction distance, H ($\overset{\circ}{A}$)	Overall Adhesion Force, F_T (N)
10	1.11×10^{-9}
20	2.7×10^{-10}
50	3.6×10^{-11}

greater for the mixed deposit than for the pure kaolin layers, leading to a more flattened secondary minimum and to a smaller energy barrier (see point 4.1.3.). Therefore, the probability of a stable adhesion at this secondary minimum is rather low on account of the weak bond forces present, which would explain the small percentage (20%) of the "loose" layer in the kaolin-magnetite deposits. However, those particles that succeed in overcoming the relatively small energy barrier will stabilize at the primary minimum where the adhesion force is supposed to be stronger (Table 2) than for the pure kaolin deposits. In short, the behaviour of the mixed deposits could be described by the existence of a certain "induction" or "delay" period before a stable adhesion is obtained but once this is achieved the result is a more compact and rigid fouling film.

It must be emphasized that the interpretation given above is no more than an attempt to show the potential applications of the studies of the physical-chemistry of surfaces on the analysis of actual fouling situations, at least from a qualitative point of view. The approach presented in this text is a very simplified one, since many other factors may affect the adhesion phenomena in the kaolin-magnetite deposits, such as: the different shapes of the two types of particles, the amphoteric nature of aluminium, the possible creation of opposite charges on the edges of kaolin particles, etc.

5. FINAL REMARKS

From a practical standpoint, the work carried out so far with kaolin and kaolin-magnetite suspensions in water showed that it is possible, at least in simple situations such as pure particulate fouling, to make some kind of useful predictions about the characteristics of the deposit build--up (the properties of the foulant fluid must be known, of course). For instance, the greater strength of the pure magnetite as well as of the kaolin-magnetite deposit could be foreseen knowing the zeta potentials of both materials and evaluating the Hamaker constants of each system.

Theoretical predictions of the rate of fouling are still not feasible in most cases, but the use of general fouling models containing two or three empirical parameters can be of some help if simulation experiments are conducted with carefully chosen operating conditions (taking also into account the geometry of the equipment), in order to evaluate those parameters.

The identification of the processes controlling the fouling rate is important because it shows the mechanisms upon which the calculations should be based. For instance, when diffusion mass transfer is the control- ling process, the prediction of fouling tendencies is facilitated by the existence of reliable mathematical tools describing that transfer phenomenon.

The analysis of the curve of the potential energy of interaction may also be an important source for the detection of the type of process controlling inorganic deposition; further investigation is needed in order

to apply the surface forces approach to the interpretation and prediction of actual fouling cases.

LIST OF SYMBOLS

A' – Hamaker constant (generic case), J
A_{ij} – Hamaker constant for the system i-j, J
A_p – particle area perpendicular to the flow, m^2
a,b – empirical parameters in Pinheiro's model
C_b – bulk suspension concentration, Kg/m^3
C_D – drag coefficient
D_p – equivalent particle diameter, m
f – friction factor
F_A – van der Waals force, N
F_H – hydrodynamic force in the rotating apparatus, N
F_R – electrostatic double-layer force, N
F_T – overall adhesion force, N
H – separation (interaction) distance, m
I_i – ionization potential of substance i, J/molecule
J_t – mass transfer flux, Kg/m^2s
K_1, K_2, K_3 proportionality constants
K_a – adhesion coefficient, m/s
K_B – Boltzmann constant, J/K
K_f – thermal conductivity fo the deposit, W/mK
K_t – transport coefficient, m/s
N_i – number of molecules of substance i per unit volume, m^{-3}
n_i – refractive index of substance i
n_{io} – number of ions i per unit volume of solution, m^{-3}
nr – number of rotations per second, s^{-1}
R_1, R_2 – radii of particles 1 and 2, m
R_o, R_i – inner and outer radii of the rotating apparatus, m
Re – Reynolds number
R_f – thermal resistance of the deposit, m^2K/W
R_f^∞ – asymptotic thermal resistance of the deposit, m^2K/W
T – fluid temperature, K
t – time, s
t_p^+ – particle dimensionless relaxation time
v – local fluid velocity, m/s
$\bar{v}$ – average fluid velocity, m/s
v^* – friction velocity, m/s
V_T – overall potential energy of interaction, J
Y – distance normal to the deposition surface, m
Y_c – half-thickness of the particle, m
Y_f – thickness of the deposit, m
z_i – valency of ion i
α_i – polarizability of substance i, m^3
β – parameter related to the cohesiveness of the deposit, s^{-1}
ε – dielectric constant, $(Coulomb)^2/Nm^2$
δ – thickness of the electrostatic double-layer, m

$\emptyset_d$ – deposition flux, in termal units, m^2K/J
$\emptyset_r$ – removal flux, in thermal units, m^2K/J
$\emptyset_t^r$ – particle transport flux, in thermal units, m^2K/J
Ψ_{oi} – zeta potential of substance i, V
ρ – fluid density, Kg/m^3
ρ_f – density of the deposit, Kg/m^3
ρ_p – particle density, Kg/m^3
μ – dynamic viscosity, Ns/m^2
υ – kinematic viscosity, m^2/s
τ_w – wall shear stress on the inner tube of the rotating apparatus, N/m^2
(τ_w)h.e. – wall shear stress in the annular heat exchanger, N/m^2
ω – angular velocity of the rotating apparatus, s^{-1}

REFERENCES

1 . Melo,L.F. and J.D. Pinheiro, "Particulate fouling: controlling processes and deposit strucutre", 8th Intern. Heat Transfer Conf., Vol. 6, Paper HX-16,2781-2786, S. Francisco, USA, 1986.
2 . Kern, D. and R. Seaton, "A theoretical analysis of thermal surface fouling", Brit. Chem. Engin., 4(5), 258-262, 1959.
3 . Pinheiro, J.D., "Fouling of heat transfer surfaces", in "Heat exchangers: Thermal-Hydraulic Fundamentals and Design", Ed. byKakaç, Bergles and Mayinger, 1013-1033, McGraw-Hill, 1981.
4 . Pinheiro, J.D., "Fouling of heat exchangers – discussion of a model", Intern. Semin. Advanc. in Heat Exchangers, Intern. Center of Heat and Mass Transfer, Dubrovnik, Yoguslavia, 1981.
5 . Taborek, J., Aoki, T., Ritter, R.B.Palen, J.W. and J.G. Knudsen,"Fouling: the major unresolved problem in heat transfer", Chem. Eng. Progr., 68(2) 59-67, 1972.
6 . Watkinson, A.P. and N. Epstein, "Gas oil fouling in a sensible heat exchanger", Chem. Eng. Progr. Sump. Ser., 65(92), 84-90, 1969.
7 . Crittenden, B. and S.T. Kolackzkowski, "Energy savings through accurate prediction of heat transfer fouling resistance", in "Energy for industry" Ed. by O'Callaghan, 257-260, Pergamon, Oxford, 1979.
8 . Melo, L. and J.D. Pinheiro, "Hydrodynamic effects on particulate fouling", I. Chem. Engrs. Symp. Ser., No. 86. Vol.1, 381-390, 1984.
9 . Melo, L. and J.D. Pinheiro, "Particle transport in fouling caused by kaolin-water suspensions on copper tubes", to be published in Can. J. Chem. Eng., Vol. 65, Dec. 1987.
10. Watkinson, A.P., Louis, L. and R. Brent, "Scaling of heat exchanger tubes", Can. J. Chem. Eng., 52, 558-562, 1974.
11. Watkinson, A.P. and O. Martinez, "Scaling of heat exchanger tubes by calcium carbonate", J. Heat Transfer, 504-508, 1975.
12. Wood, N.B., "A simple method for the calculation of turbulent deposition to smooth and rough surfaces", J. Aerosol Sci., 12(3), 275-290, 1981.
13. Davies, C.N., "Deposition of aerosols from turbulent flow through pipes", Proc. Roy. Soc. London, Ser. A, 289, 235-246, 1966.
14. Davies, C.N., "Brownian deposition of aerosol particles from turbulent flow through pipes", Proc. Roy. Soc. London, Ser. A., 290, 557-562,1966.
15. Shaw, D.J., "Introd. to Colloid and Surface Chemistry", Butterworths, London, 1980.
16. Visser, J., "The adhesion of colloidal particles to a planar surface in aqueous solutions", Ph.D. Thesis, London, 1973.
17. Visser, J., "The adhesion of colloidal polystyrene particles to cellophane as a function of pH and ionic strength", J. Coll. Interf.Sci., 55(3), 664-667, 1976.

18. Visser, J., "Adhesion and removal of particles - I and II", in "Fouling Science and Technology", Ed. by Melo, Bott and Bernardo, Kluwer Academic Publishers, 1988.
19. Barrow, G.M., "Physical Chemistry", 2nd Ed., McGraw-Hill, 1966.
20. Hogg, R., Healy, T.W. and D.W. Fuerstenau, "Mutual coagulation of colloidal dispersions", Transf. Faraday Soc., 62, 1638-1651,1966.
21. Ruckenstein, E. and D.G. Kalthod, "Role of hydrodynamics and physical interactions in the absorption and desorption of hydrosols or globular proteins", in "Fundam. and Appl, of Surf. Phenom. Assoc. with Fouling and Cleaning in Food Processing", 115-147, Univ. Lund, Sweden, 1981.
22. Ruckenstein, E. and D. Prieve, "Absorption and desorption of particles and their chromatographic separation", AICHE J., 22(2), 276-283, 1976.
23. Schubert, H., "Particle adhesion to solid surfaces", in "Fundam. and Appl. of Surf. Phenom. Assoc. with Fouling and Cleaning in Food Processing", 57-75, Univ. Lund, Sweden, 1981.
24. Rajagopalan, R. and J.S. Kim, "Adsorption of brownian particles in the presence of potential barriers: effect of different modes of double--layer interaction", J. Coll. Interf. Sci., 83(2), 428-448, 1981.
25. Prieve, D. and E. Ruckenstein, "Double-layer interaction between dissimilar ionizable surfaces and its effect on the rate of deposition", J. Coll. Interf. Sci., 63(2), 317-329, 1978.
26. Wendt, F., "Turbulent Strömungen zwischen zwei rotierenden konaxialen Zylindern", ing.-Arch., 4, 577-595, 1933.
27. Van den Tempel, M., "Interaction forces between condensed bodies in contact", Adv. Coll. Interf. Sci., 3, 137-159,
28. Grim, R.E., "Clay Mineralogy", 2nd Ed., McGraw-Hill, 1968.
29. Norrish, K., "The swelling of montmorillonite", Disc. Faraday Soc., 18, 120-134, 1954.